Supplementary Information

Freestanding Functional Structures by Aerosol-Jet Printing for Stretchable Electronics and Sensing Applications

Qingshen Jing, Yeon Sik Choi, Michael Smith, Canlin Ou, Tommaso Busolo,

*Sohini Kar-Narayan**

E-Mail: sk568@cam.ac.uk

Keywords: Aerosol jet printing, stretchable electronics, strain sensor, humidity sensor

Supplementary Note N1

To estimate the volume ratio between polyimide and Ag in the aerosol mixture, we conducted two individual ink accumulation tests, where all the parameters and set-ups were the same as normal mixing printing, with only one of the ink jar/vial filled with inks each time. That means only one ink was printed in the mixed printing process with the other ink replaced by air. Empty sample collectors were placed under the printer's head, where materials were collected until the mass is significant enough to weight (around 30 minutes). The printing mass rate can be then calculated for each ink individually to estimate the ratio of the two inks when being printed together.

Supplementary Figure S1-S13

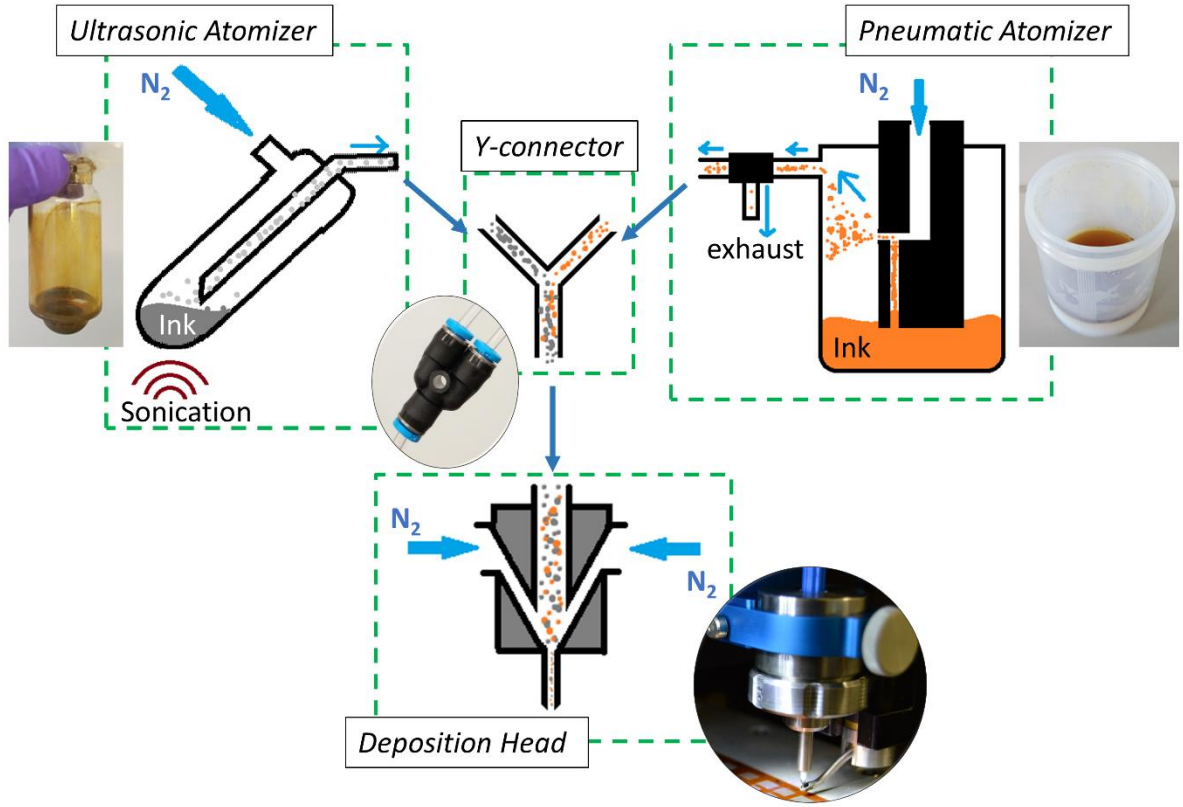

Figure S1. Schematic showing the different steps involved in aerosol jet printing: atomizing, carrying, mixing and depositing the inks in atomizers, Y-connector and deposition head, respectively.

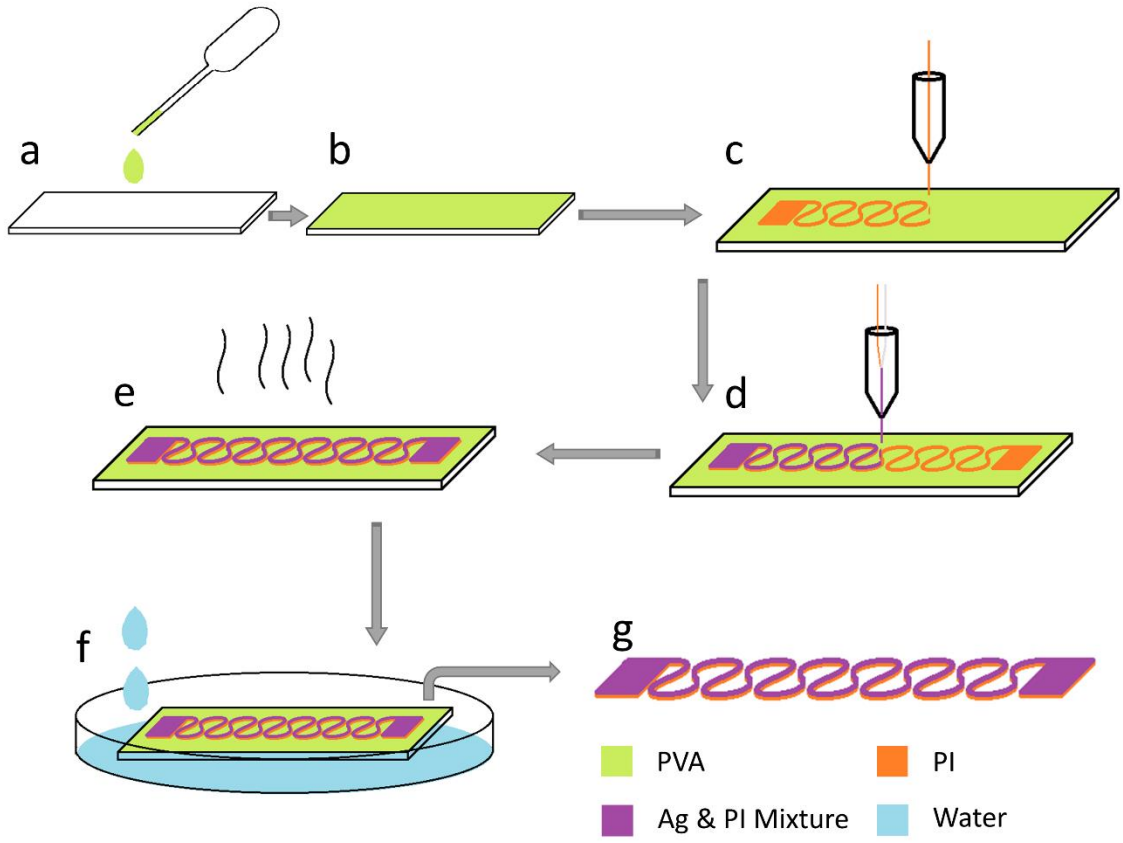

Figure S2. The complete process of fabrication of the FSCW. a) & b) PVA is spin-coated on the glass substrate. c) Polyimide is firstly printed into serpentine structure. d) Conductive Ag and PI ink is then printed with the same path over polyimide pattern. e) Sample is cured. f) Sample is placed into the water to dissolve PVA. g) Sample is lifted as FSCW.

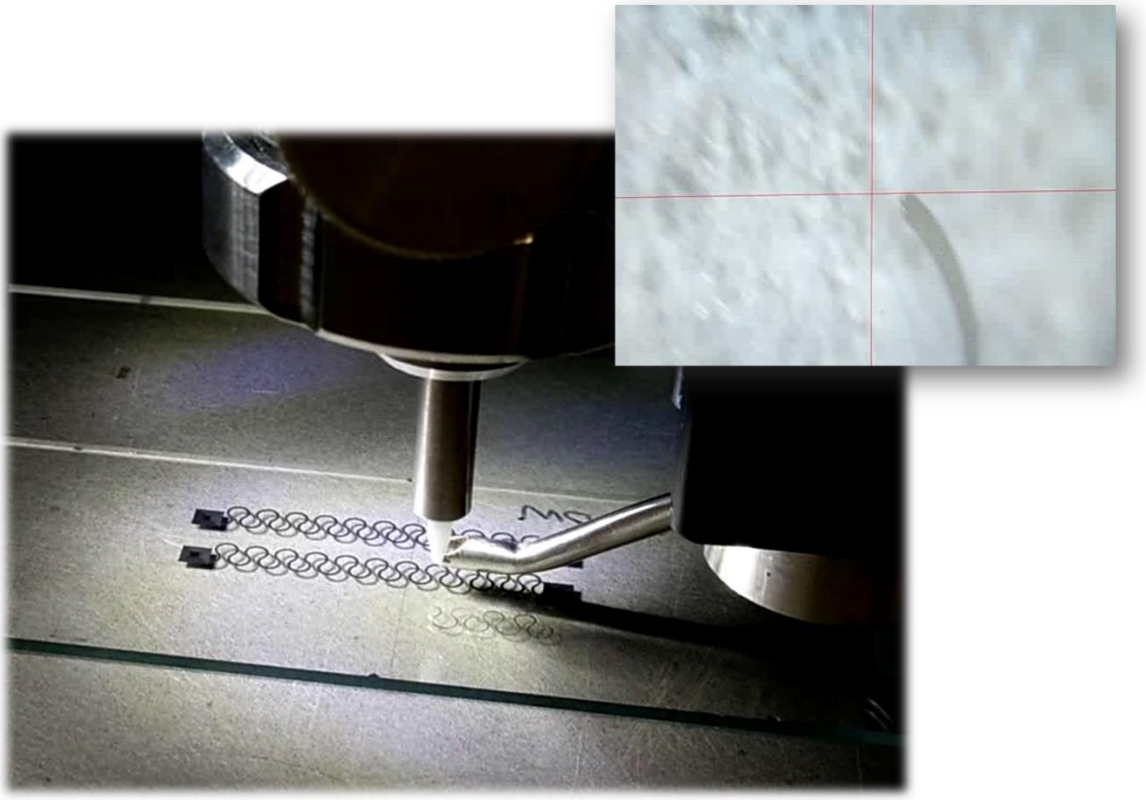

Figure S3. A photo showing the printing process of the aerosol jet printer at deposition head (bottom left) and monitoring camera (top right). There is also a Movie S1 showing the process.

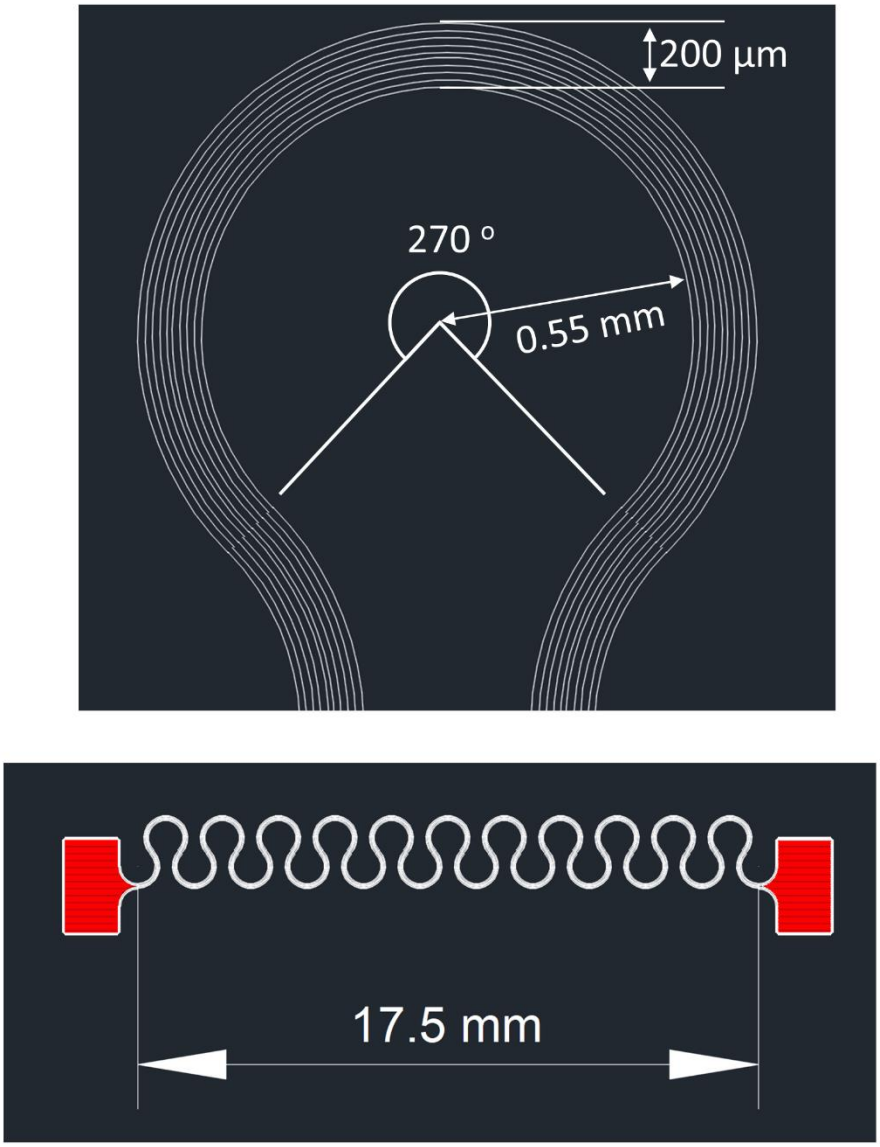

Figure S4. AutoCAD graphs showing the dimensions of the designed FSCW for AJP.

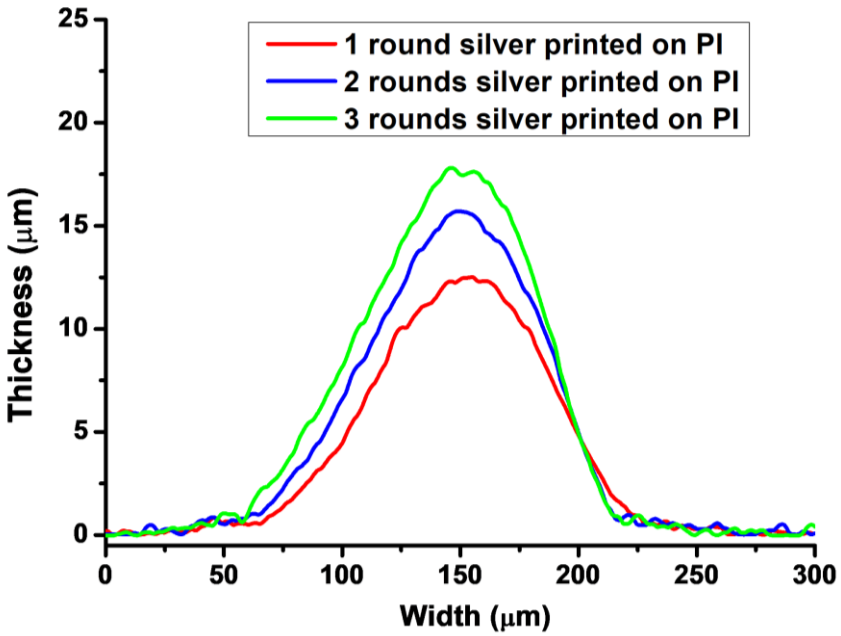

Figure S5. Thickness of wires with different layers of material being printed (counted by rounds of printing as each round of printing may contain overlapped paths), characterized by Dektak 6M stylus profilometer.

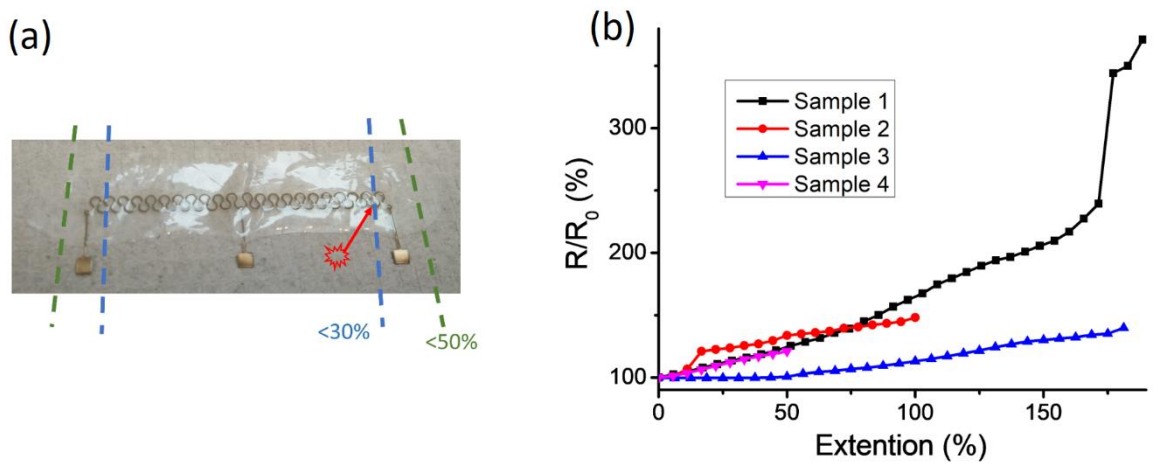

Figure S6. (a) A stretchable wire embedded in a polyurethane thin-film is conducted in stretchability test, where if the mounting position is at the blue dash line shown in the figure, the wire would fail at 30 % stretching at the position of the mounting point. If the mounting position is at the green line, the wire would fail at 50%, slightly better but not as good as when the wire is free from substrates. (b) Variation in resistance as a function of extension in multiple free-standing conductive wire samples. Samples 1 and 3 were tested to the point of breaking. The others were not tested till breaking point as these were used later as strain sensors. The slight increase in resistance at ~10% in Sample 2 was due to the development of cracks in this sample. Each FSCW required individual calibration for strain sensing applications.

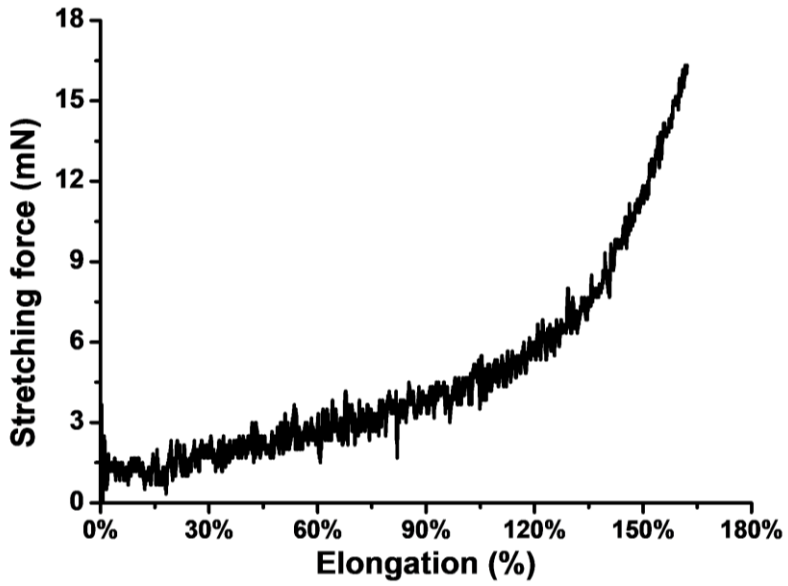

Figure S7. Mechanical test on the FSCW showing the force being applied at the ends of the wire over the elongation of the wire.

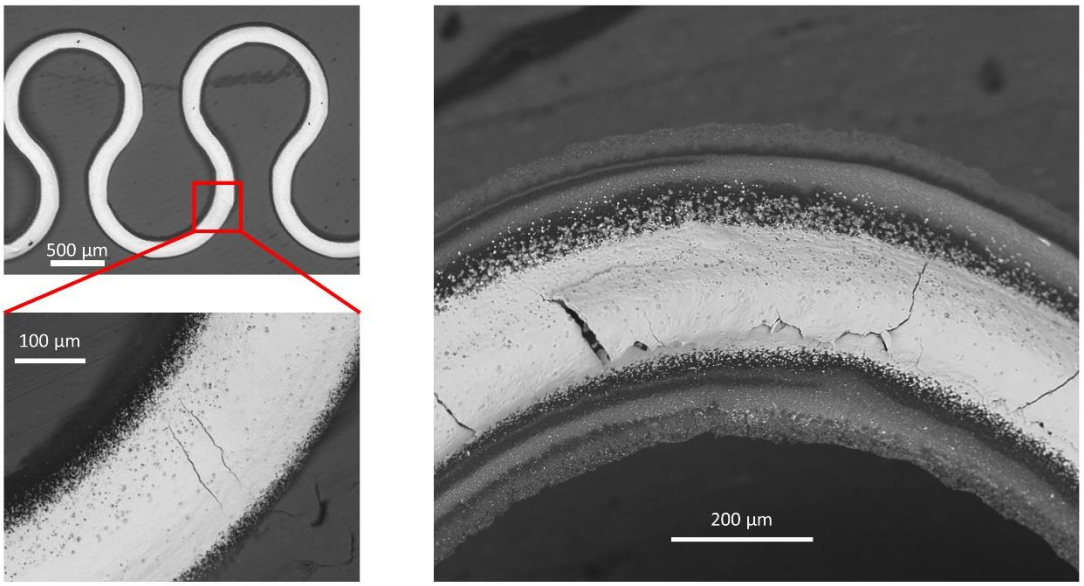

Figure S8. SEM images on the left show cracks appeared on the surface of the Ag/PI mixed layers after a few times of stretching. SEM image on the right shows material peeling off after prolonged fatigue testing.

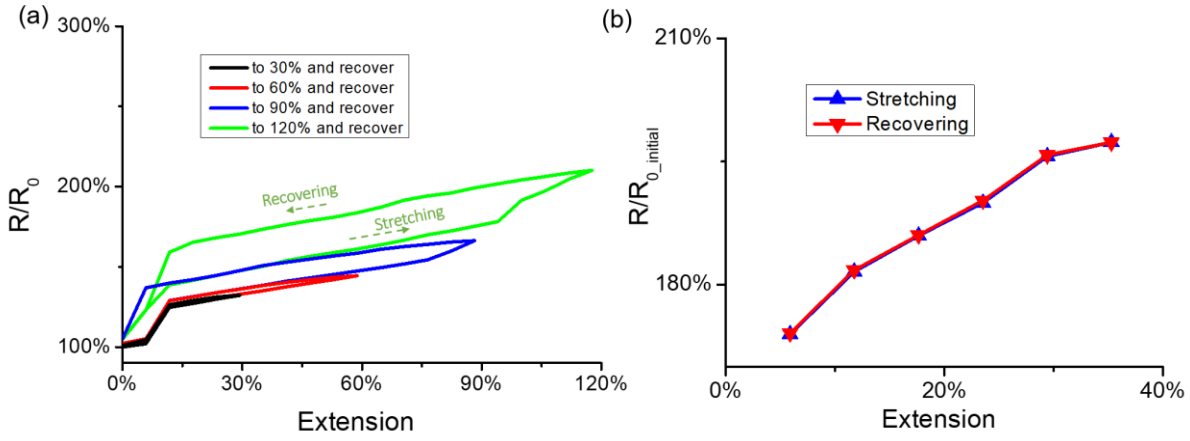

Figure S9. Resistance changes due to stretch-and-release cycles. (a) Initially, there is little hysteresis for extensions up to 30%. Hysteresis begins to appear for larger extensions. (b) In the region of operation, after multiple stretch-and-release cycles, there was no hysteresis observed in the resistance change.

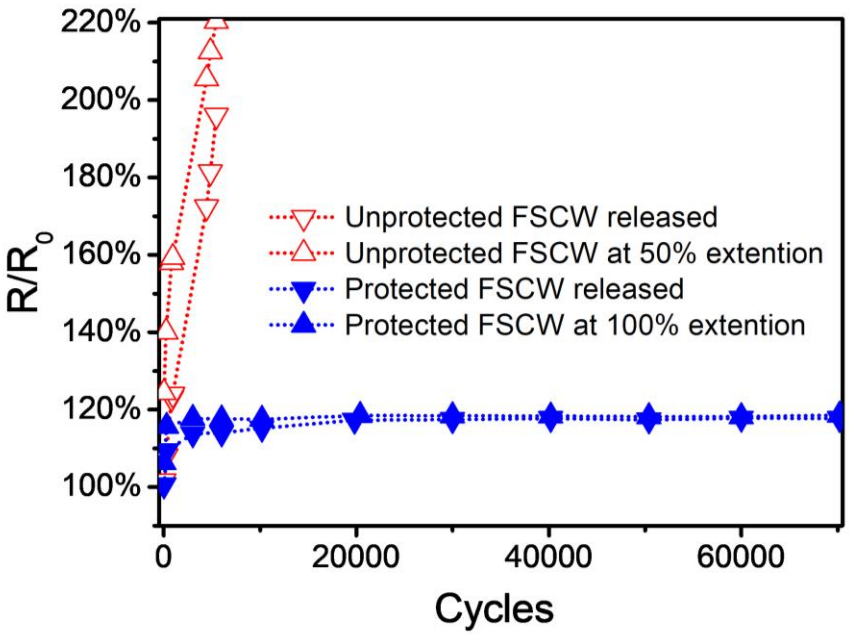

Figure S10. A comparison of resistance changes in fatigue test between protected and unprotected FSCWs. (Unprotected: Ag/PI mixture layer on top of the PI support layer was left exposed. Protected: Ag/PI mixture layer was covered by PI support layer on both sides.) Here R_0 presents the initial resistances of FSCWs at their original lengths. During the fatigue test, after a certain length of periodic stretching, resistances were measured at both released and stretched states.

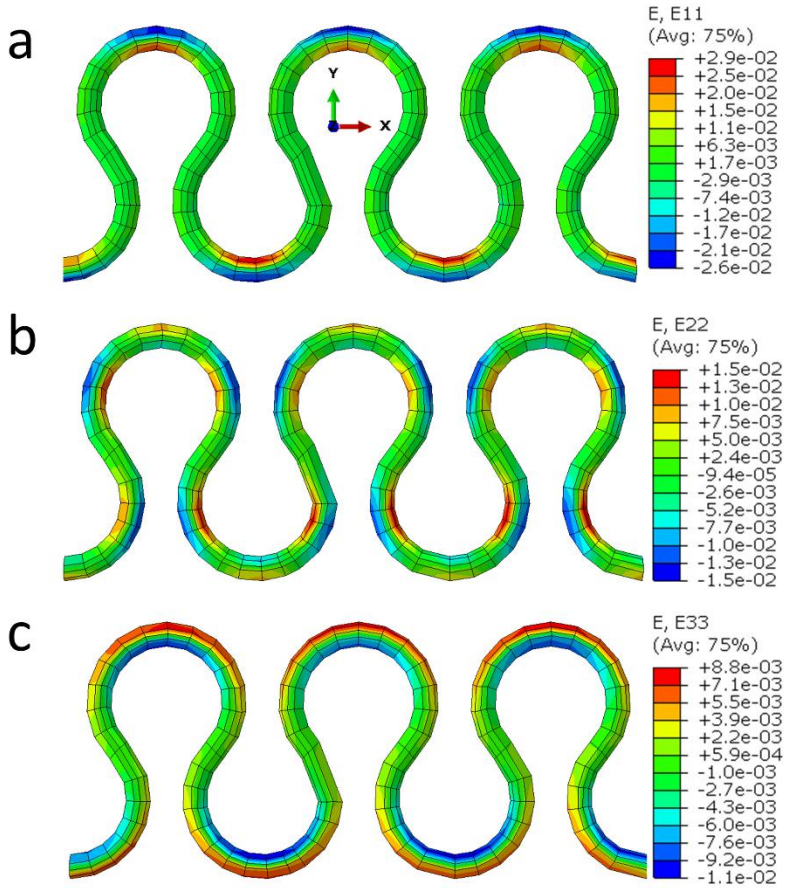

Figure S11. A finite element simulation on the stain distribution of the wire at 80% elongation shows that the normal strain of x, y and z directions (a) – (c) are concentrated at the edge of the wire, which will put little influence on capacitance.

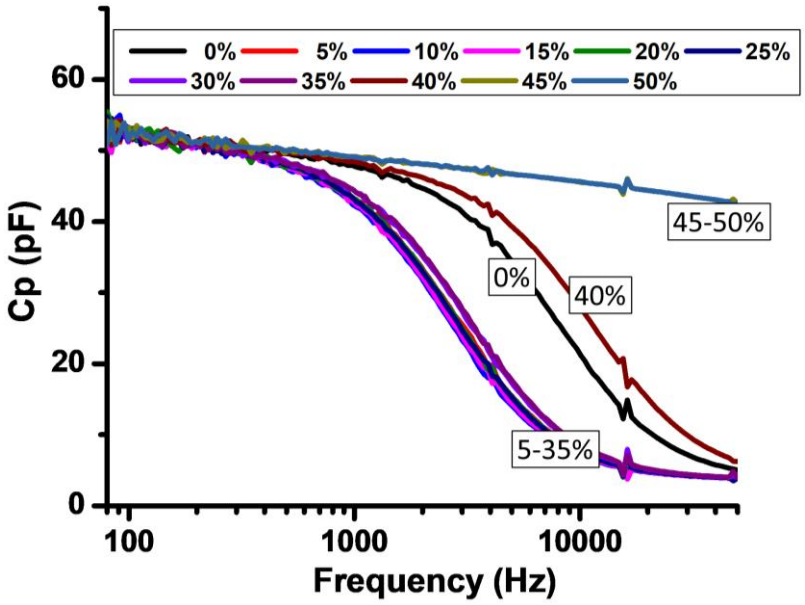

Figure S12. The capacitance of the FSCW monitored over stretching at ambient condition. The capacitance does not change much within 0-40 % elongation range. Especially at a stretching range from 5 % to 35 %.

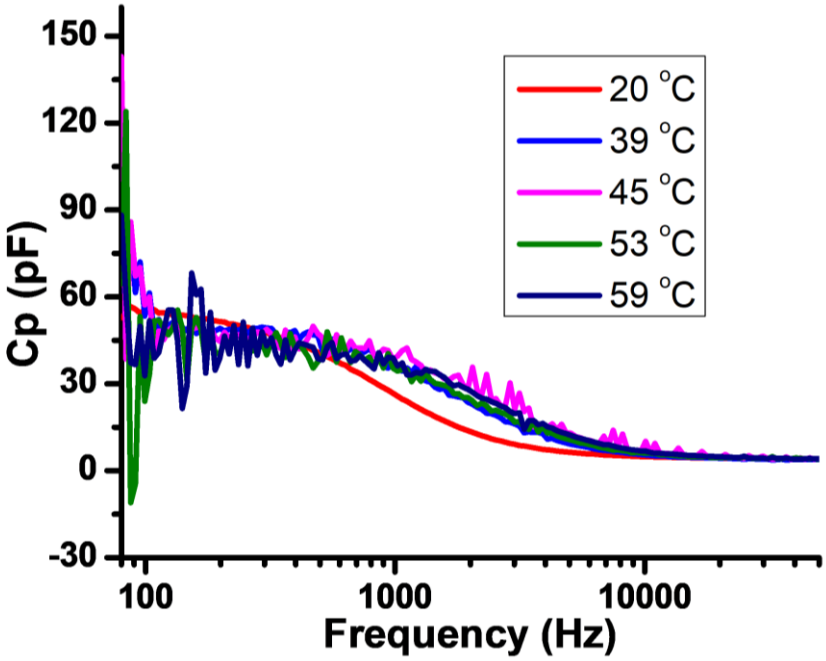

Figure S13. The capacitance of the FSCW monitored over temperature, where it does change much at the tested temperature range.